

# A measure of the size of the magnetospheric accretion region in TW Hydrae.

GRAVITY Collaboration: R. Garcia Lopez<sup>1,2,3</sup>, A. Natta<sup>2</sup>, A. Caratti o Garatti<sup>1,2,3</sup>, T.P. Ray<sup>2</sup>, R. Fedriani<sup>2,16</sup>, M. Koutoulaki<sup>2,7</sup>, L. Klarmann<sup>3</sup>, K. Perraut<sup>15</sup>, J. Sanchez-Bermudez<sup>3,18</sup>, M. Benisty<sup>15,13</sup>, C. Dougados<sup>15</sup>, L. Labadie<sup>4</sup>, W. Brandner<sup>3</sup>, P.J.V. Garcia<sup>5,6,10</sup>, Th. Henning<sup>3</sup>, P. Caselli<sup>8</sup>, G. Duvert<sup>15</sup>, T. de Zeeuw<sup>8,14</sup>, R. Grellmann<sup>4</sup>, R. Abuter<sup>7</sup>, A. Amorim<sup>6,17</sup>, M. Bauböck<sup>8</sup>, J.P. Berger<sup>7,15</sup>, H. Bonnet<sup>7</sup>, A. Buron<sup>8</sup>, Y. Clénet<sup>9</sup>, V. Coudé du Foresto<sup>9</sup>, W. de Wit<sup>10</sup>, A. Eckart<sup>4,11</sup>, F. Eisenhauer<sup>8</sup>, M. Filho<sup>5,6,10</sup>, F. Gao<sup>8</sup>, C.E. Garcia Dabo<sup>7</sup>, E. Gendron<sup>9</sup>, R. Genzel<sup>8,12</sup>, S. Gillessen<sup>8</sup>, M. Habibi<sup>8</sup>, X. Haubois<sup>10</sup>, F. Haussmann<sup>8</sup>, S. Hippler<sup>3</sup>, Z. Hubert<sup>15</sup>, M. Horrobin<sup>4</sup>, A. Jimenez Rosales<sup>8</sup>, L. Jocou<sup>15</sup>, P. Kervella<sup>9</sup>, J. Kolb<sup>10</sup>, S. Lacour<sup>9</sup>, J.-B. Le Bouquin<sup>15</sup>, P. Léna<sup>9</sup>, T. Ott<sup>8</sup>, T. Paumard<sup>9</sup>, G. Perrin<sup>9</sup>, O. Pfuhl<sup>7</sup>, A. Ramirez<sup>7</sup>, C. Rau<sup>8</sup>, G. Rousset<sup>9</sup>, S. Scheithauer<sup>3</sup>, J. Shangguan<sup>8</sup>, J. Stadler<sup>8</sup>, O. Straub<sup>8</sup>, C. Straubmeier<sup>4</sup>, E. Sturm<sup>8</sup>, E. van Dishoeck<sup>8,14</sup>, F. Vincent<sup>9</sup>, S. von Fellenberg<sup>8</sup>, F. Widmann<sup>8</sup>, E. Wieprecht<sup>8</sup>, M. Wiest<sup>4</sup>, E. Wiezorrek<sup>8</sup>, J. Woillez<sup>7</sup>, S. Yazici<sup>8,4</sup> & G. Zins<sup>10</sup>

<sup>1</sup>*School of Physics, University College Dublin, Belfield, Dublin 4, Ireland*

<sup>2</sup>*Dublin Institute for Advanced Studies, 31 Fitzwilliam Place, D02 XF86 Dublin, Ireland*

<sup>3</sup>*Max Planck Institute for Astronomy, Königstuhl 17, Heidelberg, Germany, D-69117*

<sup>4</sup>*I. Physikalisches Institut, Universität zu Köln, Zùlpicher Str. 77, 50937, Köln, Germany*

<sup>5</sup>*Faculdade de Engenharia, Universidade do Porto, Rua Dr. Roberto Frias, P-4200-465 Porto, Portugal*

<sup>6</sup>*CENTRA, Centro de Astrofísica e Gravitação, Instituto Superior Técnico, Avenida Rovisco Pais 1, P-1049 Lisboa, Portugal*

<sup>7</sup>*European Southern Observatory, Karl-Schwarzschild-Str. 2, 85748 Garching, Germany*

<sup>8</sup>*Max Planck Institute for Extraterrestrial Physics, Giessenbachstrasse, 85741 Garching bei München, Germany*

<sup>9</sup>*LESIA, Observatoire de Paris, Université PSL, CNRS, Sorbonne Université, Université de Paris, 5 place Jules Janssen, 92195 Meudon, France*

<sup>10</sup>*European Southern Observatory, Casilla 19001, Santiago 19, Chile*

<sup>11</sup>*Max-Planck-Institute for Radio Astronomy, Auf dem Hügel 69, 53121 Bonn, Germany*

<sup>12</sup>*Department of Physics, Le Conte Hall, University of California, Berkeley, CA 94720, USA*

<sup>13</sup>*Unidad Mixta Internacional Franco-Chilena de Astronomía (CNRS UMI 3386), Departamento de Astronomía, Universidad de Chile, Camino El Observatorio 33, Las Condes, Santiago, Chile*

<sup>14</sup>*Sterrewacht Leiden, Leiden University, Postbus 9513, 2300 RA Leiden, The Netherlands*

<sup>15</sup>*Univ. Grenoble Alpes, CNRS, IPAG, F-38000 Grenoble, France*

<sup>16</sup>*Department of Space, Earth & Environment, Chalmers University of Technology, SE-412 93 Gothenburg, Sweden*

<sup>17</sup>*Universidade de Lisboa - Faculdade de Ciências, Campo Grande, P-1749-016 Lisboa, Portugal*

<sup>18</sup>*Instituto de Astronomía, Universidad Nacional Autónoma de México, Apdo. Postal 70264, Ciudad de México, 04510, México*

**Stars form by accreting material from their surrounding disks. There is a consensus that matter flowing through the disk is channelled onto the stellar surface by the stellar magnetic field. This is thought to be strong enough to truncate the disk close to the so-called corotation radius where the disk rotates at the same rate as the star. Spectro-interferometric**

studies in young stellar objects show that Hydrogen is mostly emitted in a region of a few milliarcseconds across, usually located within the dust sublimation radius<sup>1-3</sup>. Its origin is still a matter of debate and it can be interpreted as coming from the stellar magnetosphere, a rotating wind or a disk. In the case of intermediate-mass Herbig AeBe stars, the fact that the  $\text{Br}\gamma$  emission is spatially resolved rules out that most of the emission comes from the magnetosphere<sup>4-6</sup>. This is due to the weak magnetic fields (some tenths of G) detected in these sources<sup>7,8</sup>, resulting in very compact magnetospheres. In the case of T Tauri sources, their larger magnetospheres should make them easier to resolve. However, the small angular size of the magnetosphere (a few tenths of milliarcseconds), along with the presence of winds<sup>9,10</sup> emitting in Hydrogen make the observations interpretation challenging. Here, we present direct evidence of magnetospheric accretion by spatially resolving the inner disk of the 60 pc<sup>11</sup> T Tauri star TW Hydrae through optical long baseline interferometry. We find that the hydrogen near-infrared emission comes from a region approximately 3.5 stellar radii ( $R_*$ ) across. This region is within the continuum dusty disk emitting region ( $R_{cont} = 7 R_*$ ) and smaller than the corotation radius which is twice as big. This indicates that the hydrogen emission originates at the accretion columns, as expected in magnetospheric accretion models, rather than in a wind emitted at much larger distance ( $>1$  au).

TW Hya belongs to an association of young stars around 8 Myr old. Its proximity to Earth, as well as its favourable pole-on orientation<sup>34</sup>, makes it an ideal candidate for protoplanetary disk studies. The disk structure of TW Hya includes a dust-depleted inner hole, as well as a series of bright rings, the closest one located at  $\sim 1$  au from the star<sup>13,34</sup>. The presence of the inner

hole as well as the small near-IR excess<sup>14,33</sup> made TW Hya the prototypical “transitional disk” where planets and/or photoevaporation are expected to be the main mechanism of disk dispersal. However, the measurement of non-negligible accretion rates ( $2.3 \times 10^{-9} M_{\odot} \text{ yr}^{-1}$ )<sup>44</sup> indicates that the inner disk region of TW Hya is still rich in gas. Further evidence of accretion is given by the detection of a near pole-on cool photospheric spot (stable over several years), coincident with the location of the main magnetic pole ( $B \approx 2.5 \text{ kG}$ ), and a region of accretion-powered excess line emission<sup>17</sup>. This suggests that accretion in TW Hya takes place mostly poleward, and that the stellar magnetic field is strong enough to magnetically truncate the inner disk at a few stellar radii from the star. This value is equivalent to a few tenths of milli-arcsecond (mas), and thus it is impossible to directly resolve the magnetospheric accretion region, even for such a nearby star, using conventional methods. This leaves spectro-interferometry as the only suitable technique up to the task.

With this aim, we conducted high-angular resolution observations of the hydrogen  $\text{Br}\gamma$  line in TW Hya using the Very Large Telescope Interferometer (VLTI) instrument GRAVITY with the four 8-m Unit Telescopes (UTs; Fig. 1). The  $\text{Br}\gamma$  line is a well-known tracer of accretion in low-mass protostars through an empirical relationship that relates the line and accretion luminosities<sup>18,19</sup>. Our interferometric measurements allowed us to probe the  $\text{Br}\gamma$  line and K-band emitting regions along six different baselines (projected baselines ranging from  $\sim 130 \text{ m}$  to  $\sim 45 \text{ m}$ , resulting in nominal angular resolutions of  $\sim 4 \text{ mas}$  to  $\sim 10 \text{ mas}$ ) and at various position angles. By fitting a geometrical model (see Methods) to the continuum emission (star plus continuum circumstellar emission) and assuming a K-band to stellar flux ratio of 1.18<sup>33,44</sup>, we derive a stellar radius

of  $R_* = 1.29 \pm 0.19 R_\odot$  (consistent with theoretical expectations) and a radius for the K-band continuum excess/circumstellar emission of  $R_{circ} = 6.50 \pm 0.16 R_*$  (see Fig. 2). These values are in agreement with previous interferometric results, and spectroscopic studies<sup>33,36,44</sup>. Furthermore, the location of the K-band excess emission is consistent with the location of a disk rim due to silicate sublimation (see Methods).

By removing the continuum contribution to the line emission (see Methods), we find that the  $\text{Br}\gamma$  line emitting region is very compact, but nonetheless, marginally resolved for the longest projected baselines ( $\text{PBL} \gtrsim 60 \text{ m}$ ). This allows us to measure a radius for the  $\text{Br}\gamma$  emitting region of  $R_{\text{Br}\gamma} = 3.49 \pm 0.20 R_*$  assuming a distance of  $\sim 60 \text{ pc}$  to TW Hya (see Fig. 2). This size is consistent with the small  $\lesssim 1^\circ$  ( $\lesssim 2^\circ$  total amplitude) photocentre shift of the line with respect to the continuum (the so-called differential phase) detected in our longest baselines (see Fig. 1). Such a differential phase roughly translates into a  $\text{Br}\gamma$  line displacement of  $\lesssim 5 R_*$  (see Methods for more details), in agreement with the value derived from the continuum-subtracted  $\text{Br}\gamma$  line visibilities.

The inferred size of the  $\text{Br}\gamma$  line emission is too compact to be emitted in a photoevaporative wind that in TW Hya is expected to be launched beyond the dust cavity ( $R > 0.5\text{-}1 \text{ au}$ , i.e.,  $R > 80\text{-}160 R_*$ )<sup>21,22</sup>. It should be pointed out that in TW Hya there is no evidence of the presence of a disk wind, which is typically emitted within  $0.5 \text{ au}$  from the source, or a jet, which would be associated with bright fast blue-shifted emission in lines such as  $\text{H}\alpha$ , and  $[\text{OI}] 6300 \text{ \AA}$ ,  $[\text{SII}] 6717 \text{ \AA}$ , that is not observed in this object<sup>9,23</sup>. Therefore, the results presented here indicate that the  $\text{Br}\gamma$  line is emitted in the magnetospheric accretion region. Classical magnetospheric accretion models

assuming free fall velocities along an axisymmetric, dipolar magnetosphere predict indeed that the  $\text{Br}\gamma$  line is formed along the accretion columns<sup>24–26</sup>. In these models, the  $\text{Br}\gamma$  line has a broad profile, comparable to the free-fall velocity, and centred around zero velocity. This is the case of the  $\text{Br}\gamma$  line observed in TW Hya that shows a full width at zero intensity (FWZI) of  $\sim 400$  km/s consistent with the expected velocity of gas around a solar mass star falling at free-fall from  $\sim 3$ - $4 R_*$ . Therefore, our measurements indicate that the  $\text{Br}\gamma$  line is emitted along the magnetospheric accretion columns that truncate the disk at around  $3.5 R_*$ .

Is this value consistent with the expected magnetospheric truncation radius of TW Hya as determined by its magnetic field? Zeeman-Doppler imaging has been used to reconstruct the magnetic field topology and strength in TW Hya<sup>17</sup>. These measurements showed that the magnetic field of TW Hya is strong ( $\sim 1.5$  kG) and mostly poloidal and axisymmetric with respect to the stellar rotation axis. The field can be separated into a complex  $\sim 2.5$  kG octupole component and a much fainter  $\sim 400$ - $700$  G dipolar large-scale field. Models for such complex magnetic field topologies show that the gas initially accretes following the dipolar field lines, although near the stellar surface the octupole component alters the flow of matter<sup>27,28</sup>. Following this idea, and the theoretical work of Bessolaz et al.<sup>29</sup>, we estimate a truncation radius of  $3$ - $4 R_*$  assuming a stellar radius and mass of  $1.22 R_\odot$  and  $0.6 M_\odot$ <sup>44</sup>, and a mass accretion rate of  $2.3 \times 10^{-9} M_\odot/\text{yr}$ <sup>33,44</sup> for TW Hya, and a strength of the dipolar magnetic field component of  $400$ - $700$  G. Therefore, the size of the  $\text{Br}\gamma$  line emitting region derived from our interferometric measurements and the size of the truncation radius estimated from the magnetic field of TW Hya are strikingly similar. In addition, the measured size of the line emission is inconsistent with a disk wind, since it is significantly smaller than

the inferred truncation radius. There is a small possibility that dust-free disk gas extends inwards of the inferred sublimation radius, and could be responsible for at least part of the line emission. However, the previously measured magnetic field strength and geometry implies a disk truncation radius consistent with the K-band continuum size. Finally, the detection of spatially-resolved line emission rules out that most of the  $\text{Br}\gamma$  emission is originated at the accretion shock near the stellar surface. A schematic view of our findings is shown in Fig. 2 in Methods. Our results are then in agreement with the topology and strength of the magnetic field and they validate the assumption that when the magnetic field of the central star is complex, the truncation radius is located closer to the central star than would be expected if the magnetic field has a dipolar morphology of similar average strength<sup>27,30</sup>.

## Bibliography

1. Kraus, S. et al. The origin of hydrogen line emission for five Herbig Ae/Be stars spatially resolved by VLTI/AMBER spectro-interferometry. Astron. Astrophys. **489**, 1157–1173 (2008).
2. Eisner, J. A. et al. Near-Infrared Interferometric, Spectroscopic, and Photometric Monitoring of T Tauri Inner Disks. Astrophys. J. **669**, 1072–1084 (2007).
3. Perraut, K. et al. A disk wind in AB Aurigae traced with  $\text{H}\alpha$  interferometry. Astron. Astrophys. **596**, A17 (2016).
4. Kurosawa, R. et al. Probing the wind-launching regions of the Herbig Be star HD 58647 with high spectral resolution interferometry. Mon. Not. R. Astron. Soc. **457**, 2236–2251 (2016).

5. Garcia Lopez, R. et al. Probing the accretion-ejection connection with VLTI/AMBER. High spectral resolution observations of the Herbig Ae star HD 163296. Astron. Astrophys. **576**, A84 (2015).
6. Caratti o Garatti, A. et al. AMBER/VLTI high spectral resolution observations of the Br $\gamma$  emitting region in HD 98922. A compact disc wind launched from the inner disc region. Astron. Astrophys. **582**, A44 (2015).
7. Hubrig, S., Carroll, T. A., Schöller, M. & Ilyin, I. The prevalence of weak magnetic fields in Herbig Ae stars: the case of PDS 2. Mon. Not. R. Astron. Soc. **449**, L118–L122 (2015).
8. Alecian, E. et al. A high-resolution spectropolarimetric survey of Herbig Ae/Be stars - I. Observations and measurements. Mon. Not. R. Astron. Soc. **429**, 1001–1026 (2013).
9. Banzatti, A. et al. Kinematic Links and the Coevolution of MHD Winds, Jets, and Inner Disks from a High-resolution Optical [O I] Survey. Astrophys. J. **870**, 76 (2019).
10. Simon, M. N. et al. Tracing Slow Winds from T Tauri Stars via Low-velocity Forbidden Line Emission. Astrophys. J. **831**, 169 (2016).
11. Bailer-Jones, C. A. L., Rybizki, J., Fouesneau, M., Mantelet, G. & Andrae, R. Estimating Distance from Parallaxes. IV. Distances to 1.33 Billion Stars in Gaia Data Release 2. Astron. J. **156**, 58 (2018).
12. Huang, J. et al. CO and Dust Properties in the TW Hya Disk from High-resolution ALMA Observations. Astrophys. J. **852**, 122 (2018).

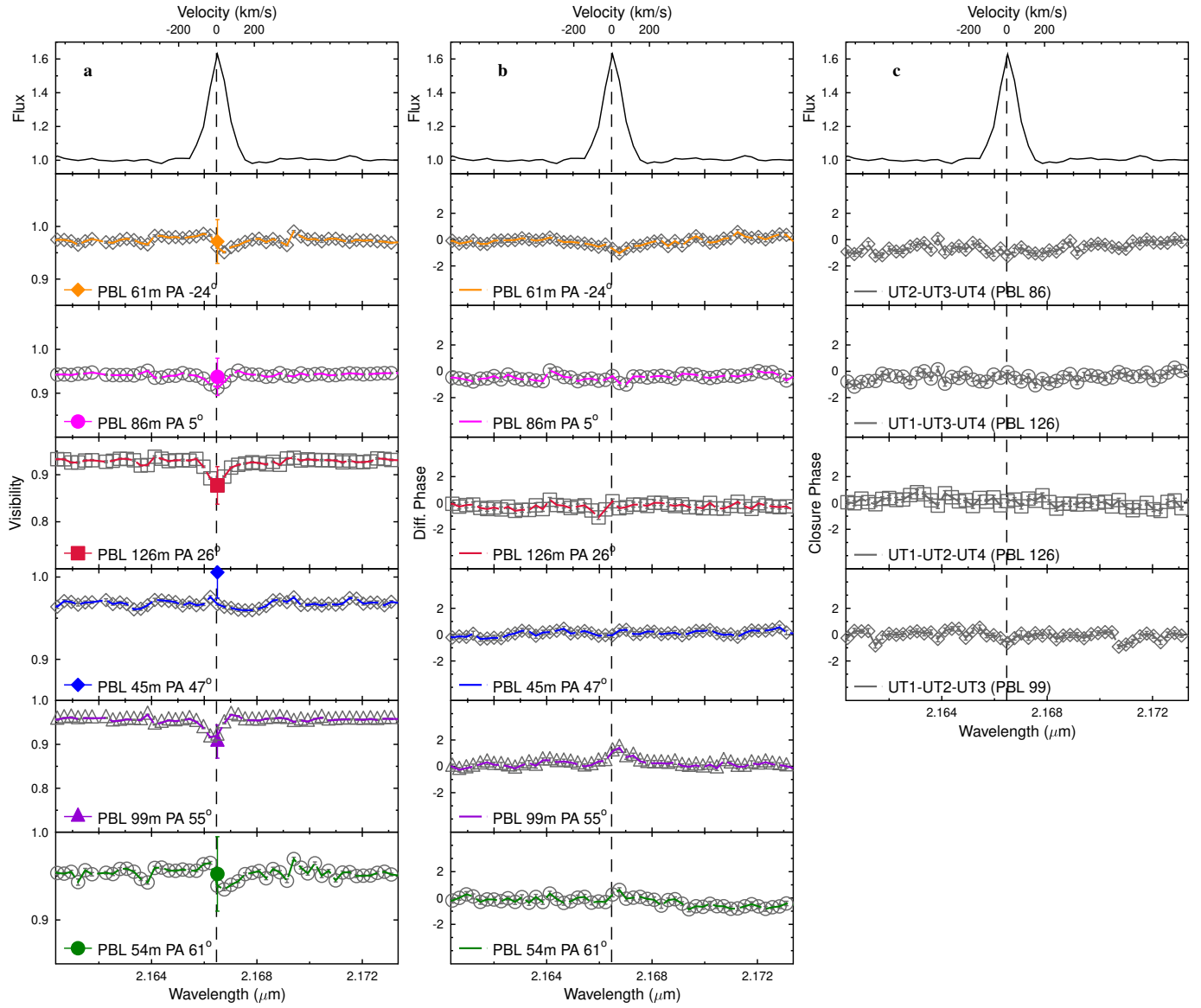


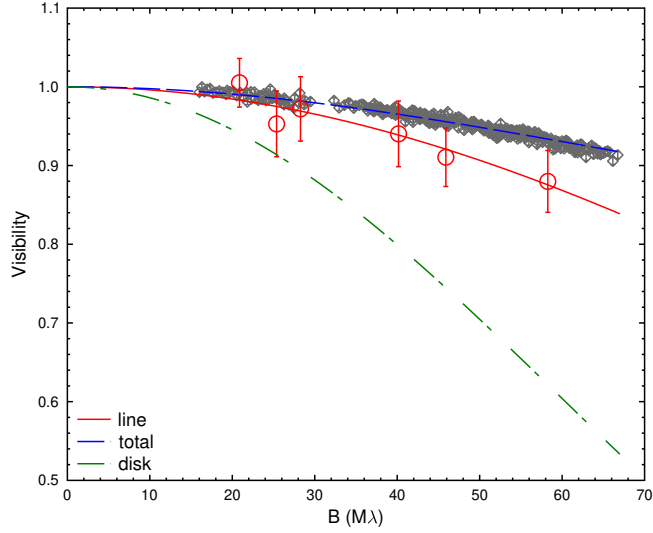
13. van Boekel, R. et al. Three Radial Gaps in the Disk of TW Hydrae Imaged with SPHERE. Astrophys. J. **837**, 132 (2017).
14. Calvet, N., et al. Evolution of Disk Accretion. Protostars and Planets IV 377–+ (2000).
15. Manara, C. F. et al. Gas content of transitional disks: a VLT/X-Shooter study of accretion and winds. Astron. Astrophys. **568**, A18 (2014).
16. Venuti, L. et al. X-shooter spectroscopy of young stars with disks. The TW Hydrae association as a probe of the final stages of disk accretion. Astron. Astrophys. **632**, A46 (2019).
17. Donati, J. F. et al. The large-scale magnetic field and poleward mass accretion of the classical T Tauri star TW Hya. Mon. Not. R. Astron. Soc. **417**, 472–487 (2011).
18. Muzerolle, J., Hartmann, L. & Calvet, N. A Br $\gamma$  Probe of Disk Accretion in T Tauri Stars and Embedded Young Stellar Objects. Astron. J. **116**, 2965–2974 (1998).
19. Alcalá, J. M. et al. X-shooter spectroscopy of young stellar objects. IV. Accretion in low-mass stars and substellar objects in Lupus. Astron. Astrophys. **561**, A2 (2014).
20. Akeson, R. L. et al. Radial Structure in the TW Hya Circumstellar Disk. Astrophys. J. **728**, 96 (2011).
21. Pascucci, I. et al. The Photoevaporative Wind from the Disk of TW Hya. Astrophys. J. **736**, 13 (2011).
22. Ercolano, B., Rosotti, G. P., Picogna, G. & Testi, L. A photoevaporative gap in the closest planet-forming disc. Mon. Not. R. Astron. Soc. **464**, L95–L99 (2017).

23. Fang, M. et al. A New Look at T Tauri Star Forbidden Lines: MHD-driven Winds from the Inner Disk. *Astrophys. J.* **868**, 28 (2018).
24. Muzerolle, J., Calvet, N. & Hartmann, L. Emission-Line Diagnostics of T Tauri Magnetospheric Accretion. II. Improved Model Tests and Insights into Accretion Physics. *Astrophys. J.* **550**, 944–961 (2001).
25. Kurosawa, R., Romanova, M. M. & Harries, T. J. Multidimensional models of hydrogen and helium emission line profiles for classical T Tauri stars: method, tests and examples. *Mon. Not. R. Astron. Soc.* **416**, 2623–2639 (2011).
26. Gullbring, E., Hartmann, L., Briceno, C. & Calvet, N. Disk Accretion Rates for T Tauri Stars. *Astrophys. J.* **492**, 323–+ (1998).
27. Gregory, S. G., Matt, S. P., Donati, J. F. & Jardine, M. The non-dipolar magnetic fields of accreting T Tauri stars. *Mon. Not. R. Astron. Soc.* **389**, 1839–1850 (2008).
28. Romanova, M. M., Long, M., Lamb, F. K., Kulkarni, A. K. & Donati, J. F. Global 3D simulations of disc accretion on to the classical T Tauri star V2129 Oph. *Mon. Not. R. Astron. Soc.* **411**, 915–928 (2011).
29. Bessolaz, N., Zanni, C., Ferreira, J., Keppens, R. & Bouvier, J. Accretion funnels onto weakly magnetized young stars. *Astron. Astrophys.* **478**, 155–162 (2008).
30. Johnstone, C. P., Jardine, M., Gregory, S. G., Donati, J. F. & Hussain, G. Classical T Tauri stars: magnetic fields, coronae and star-disc interactions. *Mon. Not. R. Astron. Soc.* **437**, 3202–3220 (2014).

Table 1: **Size estimates derived from the best fit of the continuum and continuum-compensated Br $\gamma$  line data.**

TW Hya	R	R	R
	[mas]	[au]	[R $_{\odot}$ ]
star	$0.10 \pm 0.01$	$0.006 \pm 0.001$	$1.29 \pm 0.19$
disk	$0.65 \pm 0.02$	$0.039 \pm 0.001$	$8.39 \pm 0.21$
line	$0.35 \pm 0.02$	$0.021 \pm 0.001$	$4.50 \pm 0.26$





## Methods

### 1 Observations and data reduction

TW Hya was observed with the VLTI instrument GRAVITY<sup>31</sup> on 21 January 2019 using the four 8m Unit Telescopes (UTs) of the European Southern Observatory (see Table 1 in Extended Data). The target was observed in single-field combined polarisation mode (i.e. fringes were tracked and servoed on the target itself) and operating with the MACAO on-axis adaptive optics system. The data on the fringe tracker (FT) detector were recorded at low spectral resolution ( $R \sim 23$ ) with a detector integration time per interferogram (DIT) of 0.85 ms, whereas the science (SC) detector was working at high spectral resolution (HR;  $R \sim 4000$ , i.e.,  $\Delta V \sim 70 \text{ km s}^{-1}$ ) and with a DIT of 30 s.

The data were reduced using the GRAVITY pipeline version 1.3.0<sup>32</sup>. The atmospheric trans-

fer function was calibrated using the calibrators HD 91937 and HD 95470 (see Table 1 in Extended Data). The spectrum of TW Hya was obtained by averaging the HR spectra recorded in the four photometric channels. Standard telluric correction was also applied to the spectrum using HD 95470 (SpT K2/3 III) as a telluric standard star. Finally, the spectrum was flux calibrated assuming a 2MASS K-band magnitude of 7.3 for TW Hya. The wavelength calibration of the spectra was refined using several telluric absorption lines present in the spectrum. An average shift of  $\sim 4\text{\AA}$  was applied to the data.

## 2 Interferometric Observables

VLTI-GRAVITY observations of TW Hya provided us with the K-band spectrum of the source, six spectrally dispersed visibilities (that give a measure of the size of the object, with  $V=1$  indicating a point source, and  $V=0$  indicating a fully resolved object) and differential phases (that measure the photocenter shift of the line with respect to the continuum) and four closure phases (that provides a measure of the asymmetry of the continuum and/or line emission) (see Fig. 1 in the print paper).

The spectrum of TW Hya shows bright  $\text{Br}\gamma$   $2.166\ \mu\text{m}$  line emission, along with  $\text{NaI } 2.206\ \mu\text{m}$ , and  $\text{NaI } 2.209\ \mu\text{m}$ , and rovibrational CO in absorption. No interferometric signal is detected for any of these lines except the  $\text{Br}\gamma$  line. A small differential phase signature of  $2^\circ$  in the  $\text{Br}\gamma$  line is detected along the two longest baselines. No closure phases were detected within the errors.

The continuum visibilities point towards a very compact circumstellar environment around TW Hya with measured continuum visibilities above  $\sim 0.95$  in all our baselines. Interestingly, the total visibilities within the line decreases with respect to the continuum visibilities, indicating that

the sum of the Br $\gamma$  emitting region plus the continuum contribution (including the stellar plus circumstellar environment) is more extended than the continuum alone. However, it should be noted that the total visibility is not just the sum of each visibility component but it is weighted by the flux of each component. In other words, assuming that the level of the continuum within and outside the line is the same and that the differential phase is zero then:  $V_{tot} F_{tot} = V_{cont} F_{cont} + V_{line} F_{line}$ , with  $V_{cont} F_{cont} = V_* F_* + V_{circ} F_{circ}$ ; and  $F_{tot} = F_{cont} + F_{line}$ . In these expressions,  $F_{tot}$ ,  $F_{cont}$ ,  $F_{line}$ , and  $V_{tot}$ ,  $V_{cont}$ ,  $V_{line}$  are the total, continuum and line fluxes, and visibilities respectively; and  $F_*$ ,  $F_{circ}$ , and  $V_*$ ,  $V_{circ}$  are the stellar and circumstellar continuum fluxes, and visibilities. In order to further investigate the circumstellar and Br $\gamma$  line emitting region the contribution from the star and the overall continuum emission must be removed from the measured visibilities.

### 3 Circumstellar continuum emitting region

As mentioned above, in order to estimate the size of the continuum circumstellar emitting region the emission from the star must be removed. In doing so, a K-band to stellar flux ratio of 1.18 was assumed<sup>33</sup>. As we expect to marginally resolve TW Hya due to its close distance (i.e.  $V_* < 1$  on our longest baselines), we took the conservative approach of fitting two Gaussian components to the continuum visibilities measured by GRAVITY, one corresponding to the central star plus an additional component due to the circumstellar disk (assumed to be inclined, that is, the inclination and position angle were allowed to be free parameters). Using this approach, our best fitting model corresponds to two Gaussians with full-width-at-half-maximum (FWHM) of  $FWHM_* = 0.20 \pm 0.03$  mas and  $FWHM_{circ} = 1.30 \pm 0.04$  mas, respectively. The inclination ( $i$ ) and position

angle (PA) of the latter component is consistent with a nearly face-on structure as reported by ALMA<sup>34</sup>. However, due to the lack of long baselines, along with the nearly face-on geometry, we cannot give stringent constraints on the  $i$  and PA of the system, and from now on we will assume ALMA measurements of  $i \sim 5^\circ$  and  $PA \sim 32^\circ$  as our fiducial values. Coming back to the size of the emitting region, the derived FWHM values correspond to a stellar radius of  $R_* = 1.29 \pm 0.19 R_\odot$  and  $R_{circ} = 8.39 \pm 0.21 R_\odot$  assuming a distance of 60 pc. The retrieved stellar and circumstellar radii are in good agreement with previous values found in the literature<sup>33,35–37</sup>. If a lower value of the observed K-band to stellar flux ratio of 1.10 is assumed<sup>38,39</sup>, it would provide a worse fit, with stellar and circumstellar radii with much larger errors, namely,  $R_* = 0.05 \pm 0.11$  mas (i.e.,  $0.68 \pm 1.42 R_\odot$ ), and  $R_{circ} = 0.70 \pm 0.13$  mas (i.e.  $9.03 \pm 1.68 R_\odot$ ).

#### 4 Continuum-subtracted Br $\gamma$ line visibilities

The size of the Br $\gamma$  line emitting region can be estimated by assuming that the total visibilities within the Br $\gamma$  line are due to the contribution of the line emitting region plus the continuum component. In this way, the pure (or continuum compensated) Br $\gamma$  line visibilities can be derived by subtracting the continuum contribution from the total line visibilities following<sup>40</sup>:

$$V_{cont} V_{tot} e^{i\phi'} = \frac{V_{cont}}{F_{cont} + F_{line}} (F_{cont} V_{cont} + F_{line} V_{line} e^{i\Delta\Phi}) \quad (1)$$

where  $\phi'$  is the differential phase in the line, and  $\Delta\Phi$  is the difference of the Fourier phases of the continuum and line components, that is  $\Delta\Phi(B/\lambda_{line}) = \Phi_{cont}(B/\lambda_{line}) - \Phi_{line}(B/\lambda_{line})$ . Thus the errors on the continuum compensated visibilities have been estimated taking into account the



error on the continuum and total visibilities (assuming the rms value as a conservative error), and the differential phase,  $\phi$ , errors.

Initially, the continuum-compensated Br $\gamma$  line visibilities were computed at three velocity channels at radial velocities of  $\sim -33 \text{ km s}^{-1}$ ,  $\sim 4 \text{ km s}^{-1}$ , and  $\sim 40 \text{ km s}^{-1}$ , and with a line-to-continuum ratio higher than 10%. For all six baselines, the continuum-compensated Br $\gamma$  line visibilities measured at each spectral channel are roughly the same within the errors. Therefore, the weighted-mean of the three pure line visibilities for each baseline was computed and used to derive the size of the Br $\gamma$  line emitting region. The average pure Br $\gamma$  line visibilities are shown in Fig. 1 and 2 in the print paper. The Br $\gamma$  line emitting region is marginally resolved only for the longest PBLs (PBL  $\gtrsim 60 \text{ m}$ ), meaning that the emitting region is very compact.

To derive the size of the Br $\gamma$  line emitting region, we computed a geometric model of the Br $\gamma$  line continuum-compensated visibilities using a Gaussian fit. As for the continuum, we fixed the inclination and position angle to the values derived by ALMA and we fitted the line visibilities with only the Gaussian FWHM as a free parameter. The best fit result is shown in Table 1 in the print paper, and it corresponds to a radius of the Br $\gamma$  line emitting region of  $R_{Br\gamma} = 0.35 \pm 0.02 \text{ mas}$  or  $R_{Br\gamma} = 4.5 \pm 0.26 R_{\odot}$ , assuming a distance of  $\sim 60 \text{ pc}$  to TW Hya.

In order to probe the effect of the assumed  $F_{tot}/F_{cont}$  flux ratio on our results, we have repeated the analysis varying this ratio by 10%. The results ( $R_{Br\gamma}^{-10\%} = 0.37 \pm 0.05 \text{ mas}$ ;  $R_{Br\gamma}^{-10\%} = 0.33 \pm 0.02 \text{ mas}$ ) are consistent with the previous one within the error bars.

## 5 Continuum-subtracted Br $\gamma$ line differential phase

As for the case of the visibilities, the contribution of the continuum to the differential phase can be removed. This type of analysis is specially useful when the measured photocentre shift of the line is weak<sup>41,42</sup>. Following<sup>40</sup>, the displacement of the photocentre of the line at any given wavelength can be derived from:

$$\sin(\Delta\phi) = \sin(\phi) \cdot \frac{|F_{tot}V_{tot}|}{|F_{line}V_{line}|} \quad (2)$$

The displacement of the photocenter of the emission at any given wavelength  $\delta$  is then:

$$\delta = -\Delta\phi \frac{\lambda}{2\pi B} \quad (3)$$

where  $B$  is the length of the baseline. The upper limit of the differential phase is  $\sim 1^\circ$ . This translates into a maximum value of  $\Delta\phi_{max}^{Br\gamma} = -6.2^\circ$ , equivalent to a maximum displacement of  $\delta_{max} \sim 3.8 R_\odot \sim 4.9 R_*$ . This value is very similar to the one derived from the continuum-subtracted visibilities.

## 6 Rim Radius

We can estimate the rim radius (or the distance from the star where silicates sublimate) using eq.11 of Dullemond et al.<sup>43</sup> under the assumption that the pressure scale height is a small fraction of  $R$ . For the temperature ( $T \sim 4000$  K) and radius ( $R \sim 1.2 R_\odot$ ) assumed here for TW Hya, a rim radius of  $R_{rim} \sim 7.5 R_*$  is found for a sublimation temperature  $T_{sub} = 1500$  K.

## 7 Corotation radius

The corotation radius depends on the stellar mass, radius, and rotation velocity. This latter is uncertain due to the low inclination of TW Hya with respect to the line of sight. Estimates of the rotation velocity ranges from  $80 \pm 34$  km/s (assuming a  $v \sin i = 7 \pm 3$  km/s<sup>44</sup> and a disk inclination of  $5^\circ$ <sup>34</sup>) to  $\sim 17.4$  km/s (assuming a rotation period of  $P = 3.56$  d<sup>45</sup>). Taking these values, and a stellar mass and radius of  $0.58 M_\odot$  and  $1.22 R_\odot$ <sup>44</sup>, we find a corotation radius of  $R_{co} \sim 6.5 - 7.1 R_*$ . The corotation radius is significantly larger than  $R_{Br\gamma}$ , supporting our hypothesis that the  $Br\gamma$  size measures the radius of the magnetosphere, most likely tracing the width of the region containing accretion columns.

## Bibliography

31. Gravity Collaboration et al. First light for GRAVITY: Phase referencing optical interferometry for the Very Large Telescope Interferometer. Astron. Astrophys. **602**, A94 (2017).
32. Lapeyrere, V. et al. GRAVITY data reduction software. In Optical and Infrared Interferometry IV, vol. 9146 of Proc. SPIE., 91462D (2014).
33. Manara, C. F. et al. Gas content of transitional disks: a VLT/X-Shooter study of accretion and winds. Astron. Astrophys. **568**, A18 (2014).
34. Huang, J. et al. CO and Dust Properties in the TW Hya Disk from High-resolution ALMA Observations. Astrophys. J. **852**, 122 (2018).

35. Eisner, J. A., Chiang, E. I. & Hillenbrand, L. A. Spatially Resolving the Inner Disk of TW Hydrae. *Astrophys. J.* **637**, L133–L136 (2006).
36. Akeson, R. L. et al. Radial Structure in the TW Hya Circumstellar Disk. *Astrophys. J.* **728**, 96 (2011).
37. Sokal, K. R. et al. Characterizing TW Hydra. *Astrophys. J.* **853**, 120 (2018).
38. Eisner, J. A. et al. Time-variable Accretion in the TW Hya Star/disk System. *Astrophys. J.* **722**, L28–L32 (2010).
39. Vacca, W. D. & Sandell, G. Near-infrared Spectroscopy of TW Hya: A Revised Spectral Type and Comparison with Magnetospheric Accretion Models. *Astrophys. J.* **732**, 8 (2011).
40. Weigelt, G. et al. Near-infrared interferometry of  $\eta$  Carinae with spectral resolutions of 1 500 and 12 000 using AMBER/VLTI. *Astron. Astrophys.* **464**, 87–106 (2007).
41. Whelan, E. T., Ray, T. P., Podio, L., Bacciotti, F. & Randich, S. Classical T Tauri-like Outflow Activity in the Brown Dwarf Mass Regime. *Astrophys. J.* **706**, 1054–1068 (2009).
42. Agra-Amboage, V. et al. Origin of the wide-angle hot H<sub>2</sub> in DG Tauri. New insight from SINFONI spectro-imaging. *Astron. Astrophys.* **564**, A11 (2014).
43. Dullemond, C. P., Dominik, C. & Natta, A. Passive Irradiated Circumstellar Disks with an Inner Hole. *Astrophys. J.* **560**, 957–969 (2001).
44. Venuti, L. et al. X-shooter spectroscopy of young stars with disks. The TW Hydrae association as a probe of the final stages of disk accretion. *Astron. Astrophys.* **632**, A46 (2019).

45. Setiawan, J. et al. A young massive planet in a star-disk system. *Nature* **451**, 38–41 (2008).

**Data availability** Based on observations collected at the European Southern Observatory under ESO programme 0102.C-0408(C). The raw data are publicly available in the ESO Science Archive Facility. The reduced data that support the findings of this study are available from the corresponding author under reasonable request.

**Acknowledgements** The authors would like to thank Dr. C. Manara for kindly providing the XSHOOTER spectrum of TW Hya and the template of the stellar photosphere. This material is based upon works supported by Science Foundation Ireland under Grant No. 18/SIRG/5597. M.K. was funded by the Irish Research Council (IRC), grant GOIPG/2016/769. R.F. acknowledges support from Chalmers Initiative on Cosmic Origins (CICO) postdoctoral fellowship. A.C.G. and T.P.R. have received funding from the European Research Council (ERC) under the European Union’s Horizon 2020 research and innovation programme (grant agreement No. 743029). A.N. acknowledges the kind hospitality of DIAS. A.A., M.F. and P.J.V.G acknowledge funding by Fundação para a Ciência e a Tecnologia, with grants reference UID/FIS/00099/2013 and SFRH/BSAB/142940/2018. T.H. acknowledges support from the European Research Council under the Horizon 2020 Framework Program via the ERC Advanced Grant Origins 832428.

**Authors contributions** GRAVITY is developed in a collaboration by the Max Planck Institute for Extraterrestrial Physics, LESIA of Paris Observatory and IPAG of Université Grenoble Alpes / CNRS, the Max Planck Institute for Astronomy, the University of Cologne, the Centro Multidisciplinar de Astrofísica Lisbon and Porto, and the European Southern Observatory. Authors from these institutes contributed to the concept, design, assembly, instrumental tests, science cases, verification and implementation of GRAVITY and its subsystems, and the data reduction pipeline. P.J.V.G. conducted the observations. R.G.L., K.P. and

M.K. reduced the data. R.G.L. and M.K. analysed the data. A.N. estimated the location of the disk rim, and the corotation and truncation radius. R.F. performed the model fitting of the continuum-subtracted visibilities. R.G.L. wrote the manuscript. A.N., T.P., A.C.G. edited the manuscript. R.G.L., A.N., A.C.G., T.P.R., R.F., M.K., L.K., K.P., J.S.-B., M.B., C.D., L.L., W.B., P.J.V.G., T.H., P.C., G.D., T.Z., and R.G discussed the results and their implications, and commented on the manuscript.

**Competing Interests** The authors declare that they have no competing financial interests.

**Correspondence** Correspondence and requests for materials should be addressed to R.G.L. (email: [rebeca.garcialopez@ucd.ie](mailto:rebeca.garcialopez@ucd.ie)).

**Figure 1** VLT-GRAVITY observations of TW Hya. The  $\text{Br}\gamma$  line profile normalised to the continuum is shown in the top row. The radial velocity is with respect to the stellar reference. **a:** Wavelength-dispersed visibility amplitudes for the six baselines along with the errors derived from the data reduction. The continuum-subtracted  $\text{Br}\gamma$  line visibilities are shown as full coloured symbols. The associated errors were derived by propagating Eq. 1 in Methods as described in the text. **b:** Same as **a**, but for the wavelength-dispersed differential-phase signals. **c:** Wavelength-dispersed closure phase signals for the triplets UT2-UT3-UT4, UT1-UT3-UT4, UT1-UT2-UT4 and UT1-UT2-UT3. The maximum PBL of each baseline is indicated in between parenthesis.

**Figure 2** Visibility plot of TW Hya. Visibility points versus megalambda for the continuum calibrated FT data (open grey diamonds) and the continuum-subtracted  $\text{Br}\gamma$  line (open red circles). The fit to the total continuum and continuum-subtracted  $\text{Br}\gamma$  visibilities is shown in dashed blue and solid red lines. The circumstellar/disk visibility curve is also shown in dashed-dotted green line as reference.